Journal of Advanced Research (2014) 5, 507–523

Cairo University

Journal of Advanced Research

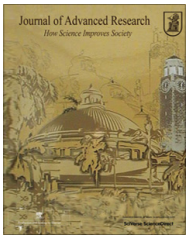

REVIEW

Fetal MRI: An approach to practice: A review

Sahar N. Saleem *

Department of Radiology, Kasr Al Ainy Faculty of Medicine, Cairo University, Cairo, Egypt

ARTICLE INFO

Article history:
Received 19 March 2013
Received in revised form 3 June 2013
Accepted 4 June 2013
Available online 11 June 2013

Keywords:
Fetal
MRI
Anomalies
Prenatal

ABSTRACT

MRI has been increasingly used for detailed visualization of the fetus in utero as well as pregnancy structures. Yet, the familiarity of radiologists and clinicians with fetal MRI is still limited. This article provides a practical approach to fetal MR imaging. Fetal MRI is an interactive scanning of the moving fetus owed to the use of fast sequences. Single-shot fast spin-echo (SSFSE) T2-weighted imaging is a standard sequence. T1-weighted sequences are primarily used to demonstrate fat, calcification and hemorrhage. Balanced steady-state free-precession (SSFP), are beneficial in demonstrating fetal structures as the heart and vessels. Diffusion weighted imaging (DWI), MR spectroscopy (MRS), and diffusion tensor imaging (DTI) have potential applications in fetal imaging. Knowing the developing fetal MR anatomy is essential to detect abnormalities. MR evaluation of the developing fetal brain should include recognition of the multilayered-appearance of the cerebral parenchyma, knowledge of the timing of sulci appearance, myelination and changes in ventricular size. With advanced gestation, fetal organs as lungs and kidneys show significant changes in volume and T2-signal. Through a systematic approach, the normal anatomy of the developing fetus is shown to contrast with a wide spectrum of fetal disorders. The abnormalities displayed are graded in severity from simple common lesions to more complex rare cases. Complete fetal MRI is fulfilled by careful evaluation of the placenta, umbilical cord and amniotic cavity. Accurate interpretation of fetal MRI can provide valuable information that helps prenatal counseling, facilitate management decisions, guide therapy, and support research studies.

Sahar N. Saleem studied medicine at Cairo University-Egypt where she earned her Master degree and Medical Doctorate in Radiology. She did Fellowships in Neuroradiology as well as in Education and Research at the University of Western Ontario-Canada. She currently works as a Professor of Radiology at Cairo University-Egypt. Saleem is specialized in advanced imaging technology. She is a pioneer in fetal Magnetic Resonance Imaging (MRI). Her achievements include proposal of the first protocol of MRI of the fetal heart, screening of fetal brain anomalies, and describing several new syndromes. Saleem has also publications in neuro-imaging, education, and studies of the mummies.

* Corresponding author.
E-mail addresses: saharsaleem1@gmail.com, saharsaleem1@ymail.com.

Peer review under responsibility of Cairo University.

2090-1232 © 2013 Production and hosting by Elsevier B.V. on behalf of Cairo University.
http://dx.doi.org/10.1016/j.jare.2013.06.001

Introduction

Although ultrasound (US) remains the predominant modality for evaluating disorders related to pregnancy, fetal MRI has been increasingly used. In contradistinction to US, MRI visualization of the fetus is not significantly limited by maternal obesity, fetal position, or oligohydramnios and visualization of the brain is not restricted by the ossified skull [1,2]. Through its superior soft tissue contrast resolution, MRI is able to distinguish individual fetal structures such as lung, liver, kidney, and bowel [3]. Moreover, MRI provides multiplanar imaging as well a large field of view, facilitating examination of fetuses with large or complex anomalies, and visualization of the lesion within the context of the entire fetal body [4]. However, fetal MRI study may give limited diagnostic information in early gestational age due to the small size of the fetus and fetal movement [5]. The purpose of this article is to provide a practical approach for radiologists and clinicians to fetal MRI performance and interpretation by adhering to guidelines. Fetal MRI technique, including recent advances, is discussed. The normal developing anatomy of the fetus and pregnancy structures is described to contrast with wide spectrum of abnormalities. Fetal MR appearance is demonstrated using different sequences. The current and future anticipated role of fetal MRI in supporting prenatal counseling, fetal therapy, and research studies are highlighted.

Fetal MRI ethics

MRI is a noninvasive diagnostic examination that does not involve ionizing radiation with no known associated negative side effects or reported delayed sequels [6]. The American College of Radiology white paper on MR safety states that pregnant patients can be accepted to undergo MR images at any stage of pregnancy if the risk-benefit ratio to the patient warrants that the study be performed [7] and only if other non-ionizing diagnostic imaging methods are inadequate. However, it is prudent to wait until 17–18th weeks of gestation before performing fetal MRI because of the potential risk to the developing fetus and the current limitations of fetal MRI created by the small size and excessive motion of younger fetuses [8]. A written informed consent is usually required from the pregnant woman prior to fetal MRI.

Indications for fetal MRI: an overview

Indications for fetal MRI include the confirmation of inconclusive sonographic findings and the evaluation of sonographically-occult diagnoses. It is unlikely that MRI will supplant US in the primary evaluation of pregnancy status and fetal well-being [1,2,5,8]. The primary indications of fetal MRI according to the recommendations of the American College of Radiology (ACR), and Society for Pediatric Radiology (SPR) [5] are included in Table 1. MRI is usually required only for a certain anatomic region, whereas a complete anatomic survey of the fetus is not required. The most common indications for fetal MRI are neurological. MRI is commonly used to investigate underlying etiologies of ventriculomegaly and morphologic brain abnormalities that are not as readily depicted with US such as dysgenesis of corpus callosum, malformations of cortical development, and posterior fossa anomalies [5,8]. Fetal MRI may detect subtle neural tube defects not shown by US and determine the level of the defect in myelomeningocele for potential fetal surgery [2,5,8,9].

The next common indication for fetal MRI is evaluation of suspicious thoracic masses. MRI has the advantage over US in differentiating the liver and bowel loops from lung tissue or masses; this aids in differentiating a congenital diaphragmatic hernia from a pulmonary mass [3]. Other indications include suspected airway obstruction caused by neck or thoracic masses. While airway can be difficult to evaluate fully with US because of artifact related to adjacent bony structures and fetal position, the fluid-filled fetal airways are well seen on T2-weighted MR images [1,3]. MRI could be helpful in providing tissue characterization of fetal abdominal masses when US study is nonspecific [1]. Because of the characteristic signal intensity of meconium, fetal MRI can distinguish marked bowel dilatation from cystic masses such as choledochal cyst and ovarian cyst [3]. MRI depicts well fetal masses in the context of whole body of the fetus in multiple planes, which may be underestimated by US because of obscuration by bony structures or fetal position [3,4].

MRI is particularly useful in the assessment of pregnancies complicated by oligohydramnios which can limit the diagnostic sensitivity of US [1,3].

Fetal MRI technique

Sequences

Development of fast MRI sequences significantly decreased fetal motion artifacts and eliminated the need for fetal sedation. A variety of fast MRI sequences are used to obtain T1- and T2-weighted images. The names and the acronyms for these sequences vary across the MR manufacturers (see Table 2). The most widely used sequence in fetal imaging is however, the single-shot fast spin-echo (SSFSE). Since SSFSE is based on single slice acquisition, fetal motion typically affects the particular slice that is being acquired while motion occurs [10].

T1-weighted images are typically acquired using two-dimensional gradient echo (2D GRE) sequences as well as a faster version of the GRE sequence called ultrafast gradient echo sequences or turbo fast low-angle shot (FLASH). Contrary to SSFSE acquisition schemes, in the gradient echo sequences all slices are acquired simultaneously. Subsequently, in the event of slight fetal movement anytime during the acquisition period, all slices are degraded by motion artifacts. In addition, spatial resolution is lower compared to SSFSE (Fig. 1) [2]. T1-weighted sequences provide little information over the T2-weighted SSFSE sequences; however, T1 weighted images are the sequence of choice for detection of hemorrhage, calcification, fat deposition and the fetal organs with high T1-hyperintensity such as thyroid and liver [8,10]. T1-weighted fat suppression images can increase the dynamic range of fetal MRI and its ability to more sensitive and specific detection of hemorrhage or fat [9]. In advanced stages of gestation, T1 weighted sequences are also used for the study of bone marrow and normal bone developmental stages [10].

Fetal MRI is also performed using balanced steady-state free precession (SSFP) sequences as balanced fast field echo (b-FFE) [11,12]. In the case of fetal brain imaging both SSFSE and b-FEE sequences provide comparable image quality especially in the 2nd trimester; however, the axonal myelination in

Table 1 Indications of fetal MRI.

Fetal organs	Indication main category	Indication sub category
Brain	Congenital anomalies	Ventriculomegaly; corpus callosal dysgenesis; holoprosencephaly; posterior fossa anomalies; malformations of cerebral cortical development
	Screening fetuses with a family risk for brain anomalies	E.g. tuberous sclerosis; corpus callosal dysgenesis; malformations of cerebral cortical development
	Vascular abnormalities	Vascular malformations; hydranencephaly; infarctions; monochorionic twin pregnancy complications
Spine	Congenital anomalies	Neural tube defects; sacrococcygeal teratomas; caudal regression/sacral agenesis; sirenomelia; vertebral anomalies
Skull, face and neck	Masses of the face and neck	Venolymphatic malformations; hemangiomas; goiter; teratomas; facial clefts
	Airway obstruction	Conditions that may impact parental counseling, prenatal management, delivery planning, and postnatal therapy
Thorax	Masses	Congenital pulmonary airway malformations (congenital cystic adenomatoid malformation; sequestration, and congenital lobar emphysema); congenital diaphragmatic hernia; effusion
	Volumetric assessment of lung	Cases at risk for pulmonary hypoplasia secondary to oligohydramnios, chest mass, or skeletal dysplasias
Abdomen, retroperitoneal and pelvis	Mass	Abdominal–pelvic cyst.; tumors (e.g. hemangiomas, neuroblastomas, sacrococcygeal teratomas, and suprarenal or renal masses); complex genitourinary anomalies (e.g. cloaca); renal anomalies in cases of severe oligohydramnios; and bowel anomalies such as megacystis microcolon
Complications of monochorionic twins		Delineation of vascular anatomy prior to laser treatment of twins; assessment of morbidity after death of a monochorionic co-twin, and improved delineation of anatomy in conjoined twins
Fetal surgery assessment		Meningomyelocele; sacrococcygeal teratomas; processes obstructing the airway (e.g. neck mass or congenital high airway obstruction); complications of monochorionic twins needing surgery; and chest masses.

N.B. The indications of fetal magnetic resonance imaging are according to the recommendations of the American College of Radiology (ACR), and Society for Pediatric Radiology (SPR) [5].

Table 2 Parameters of fetal MRI sequences.

Sequence generic names in: Philips/GE/Siemens	TR (ms)	TE (ms)	FA (degree)	NSA	Matrix	FOV (mm)	Thk/gap (mm)	Slices number	Time (s)
T1-2D GRE	120	4	70	1	166/256	300	5/0.5	15	15
T2-SSH-TSE/T2-SSFSE/HASTE	15,000	120	90	1	169/256	200–300	3–4/0–0.5	22	25
b-FFE/FIESTA/True-FISP	3.5	1.7	80	2	256×256	300–400	4–6/0	25	25
Ultrafast GRE: TFE/FMPSPGR/turbo-FLASH	7	3	20	3	200×256	300	5/0.5	14	14
DWI (b: 0 and 700 s/mm^2)	1470	125	90	1	108×256	240	5/0.1	16	19

Abbreviations: b-FFE: balanced fast field echo; DWI: diffusion weighted images; FIESTA: fast imaging employing steady-state acquisition; FLASH: fast gradient echo sequences with low flip angle shot; FMPSPGR (fast multiplanar spoiled gradient-recalled acquisition in the steady state); FOV: field-of-view; GE: general electric, medical systems Milwaukee, WI; GRE: gradient echo; HASTE: half Fourier acquired single shot turbo spin echo; mm: millimeter; ms: millisecond; NSA: number of excitations; Philips: Philips Medical Systems, Best, Netherlands; s: second; Siemens: Siemens, Erlangern, Germany; SSFP: steady state free precession; SSFSE: single shot fast spin-echo; SSH-TSE: 0.5 signal acquired single-shot half spin-echo; T1-2D GRE: T1 two dimensional gradient echo; TE: echo time ; FFE: turbo field Echo; Thk: thickness; TR: repetition time; True-FISP: fast imaging with steady precession; turbo-FLASH (fast gradient echo sequences with low flip angle shot). N.B. Modifications of the parameters may be required for different MRI systems.

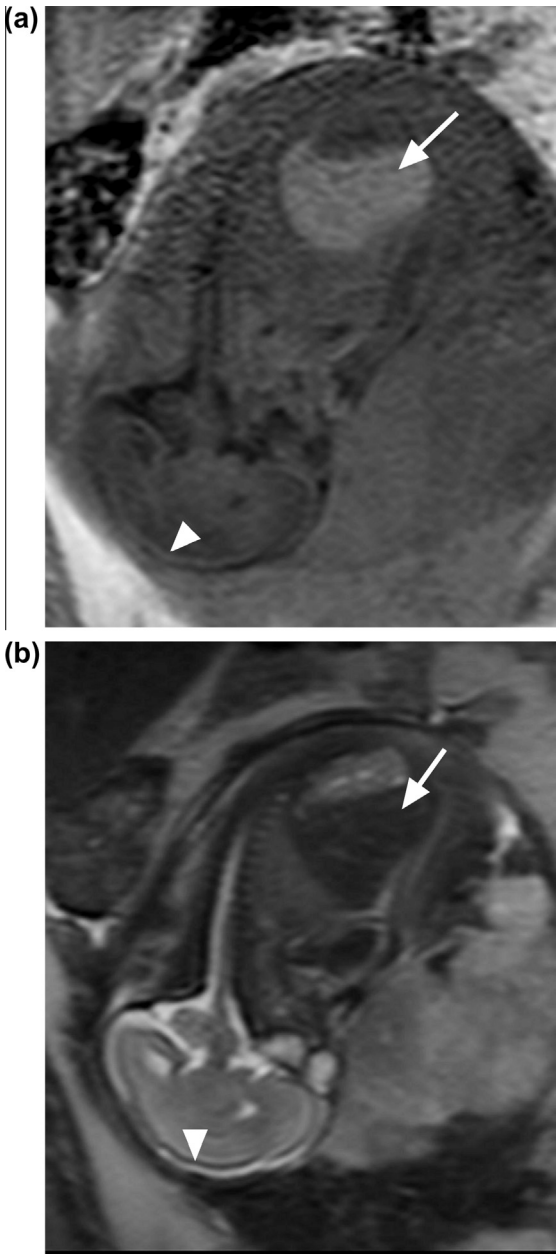

Fig. 1 Fetal MRI sequences. MR imaging of a fetus at 25 WG using T1-weighted ultrafast-gradient-echo (a) and T2-weighted SSFSE (b) sequences. The T1-weighted image has lower spatial resolution and is more prone to motion artifacts (maternal bowel peristalsis) compared to SSFSE. The liver emits high signal intensity on T1-weighted images and low signal intensity on T2-weighted images (arrows). Note that the signal of the cerebral cortex is relatively high on T1- and low on T2-weighted images (arrowheads).

the third trimester is better delineated by the latter sequence [12]. In addition, b-FEE is a preferred sequence for visualization of the fetal heart and vessels [11]. With a three times lower RF heat deposition than SSFSE sequence, b-FFE is considered to be a safer in fetal MRI [12].

Advanced MRI techniques

Advanced MRI techniques such as diffusion-weighted imaging (DWI) and magnetic resonance spectroscopy (MRS) have been

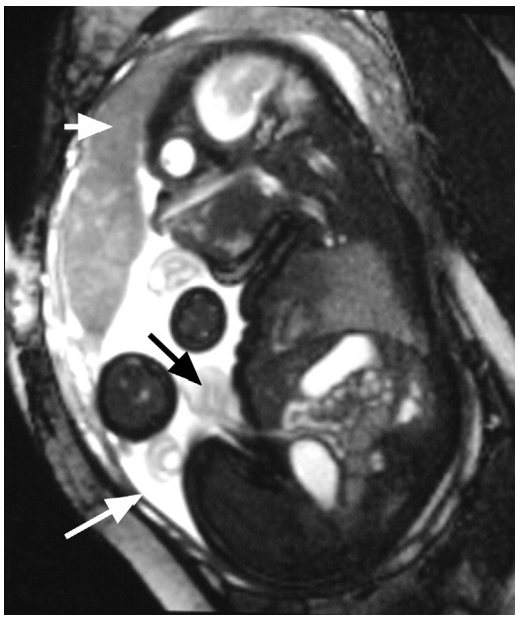

Fig. 2 Prenatal MRI evaluates the fetus and pregnancy structures. MR imaging using balanced steady state free precession sequence (b-FFE) of a gravid uterus shows well a 29 weeks old fetus and pregnancy structures: umbilical cord (black arrow), placenta (short white arrow), and amniotic sac (long white arrow). Prenatal MRI is evaluated in a system-oriented approach that includes the fetus brain, spine, face, neck, thorax, abdomen, pelvis, and extremities as well as the pregnancy structures.

applied to fetal MRI [8,10,13,14]. Diffusion imaging of the fetal brain has the potential applications for both developmental and destructive brain processes [8]. Although diffusion-tensor imaging (DTI) has been applied to fetal brain imaging; however, its clinical application is currently limited by its long acquisition times [14]. MRS imaging may provide prognostic information on brain function by assessing the risk of hypoxia through the detection of increased creatine (Cr) content [13]. Future sequences can take advantage of parallel imaging to decrease the scan time as well as increasing the signal to noise ratio (SNR) and image resolution [10,14].

Patient preparation and imaging protocols

Fetal MRI is usually performed on a 1.5 T superconducting magnet using a phased-array torso surface coil. Even with rapid image acquisition, motion can still affect the quality of the fetal MRI. Certain clinical measures can be taken to reduce motion artifacts during the study such as having the mother take nothing by mouth for at least 4 h prior the scan to prevent postprandial motion and to make sure that she empties her bladder before the study [8]. Generally the mother lies supine during the examination. In the case the mother does not tolerate the supine position. MRI can be performed in the left lateral decubitus. An initial localizer is obtained in the three orthogonal planes with respect to the mother's imaging planes, using 6–8-mm SSFSE T2-weighted sections with a 1–2-mm gap and a large field of view of (320–400 mm). Scout acquisition is used for the initial fetal visualization; for optimal signal intensity in the subsequent sequences, the fetal region of interest should be within the center of the coil. If this is not the case,

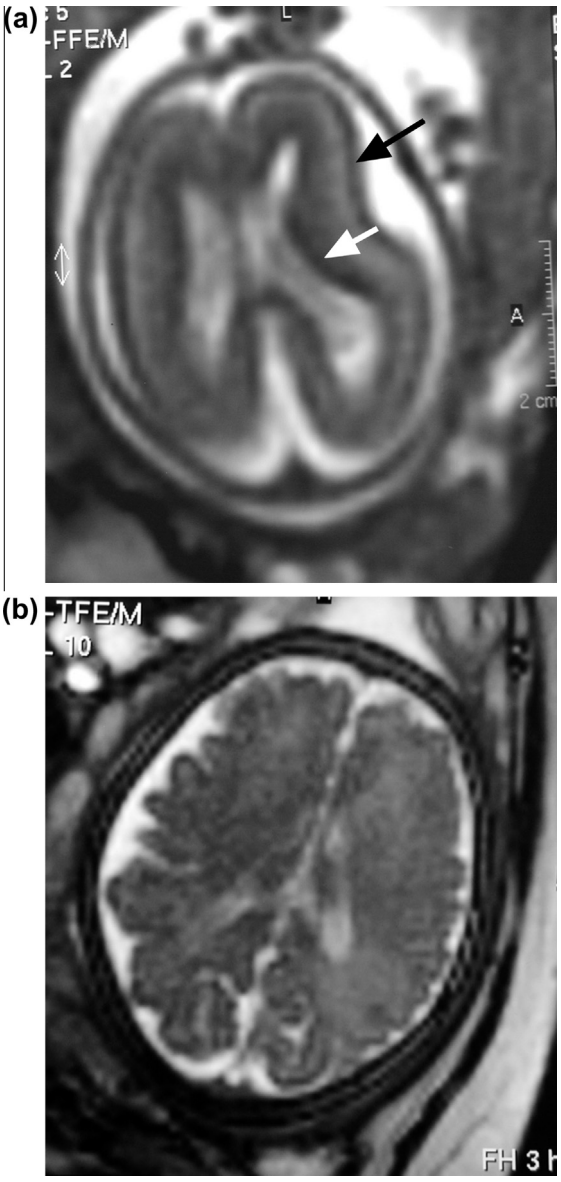

Fig. 3 Fetal brain maturation. (a) Axial b-FFE image of a fetal brain at 20 WG screened for lissencephaly (history of 2 affected siblings). The brain has a smooth surface and multilayered parenchyma: an inner dark germinal matrix (white arrow), an intermediate layer, and an outer dark developing cortex (black arrow). The ventricles and the subarachnoid spaces are prominent. On follow up MR imaging at 32 weeks of gestation (b), the fetal brain shows normal fetal brain maturation in the form of appearance of cortical sulci, disappearance of the germinal zone leaving 2 layers (the cortex and white matter), and reduction of the size of the ventricles as well as the subarachnoid space. The MRI findings helped in reassuring the expectant parents.

the coil has to be repositioned [10]. Following scout acquisition, a series of images in the axial, sagittal and coronal planes orthogonal to the fetal body region in question are obtained. Fetal MRI is an interactive scanning procedure; each acquisition serves as a scout for the subsequent one in order to avoid misregistration caused by fetal movement.

Imaging protocols have to be adapted to the suspected pathology as well as the gestational age. When evaluating

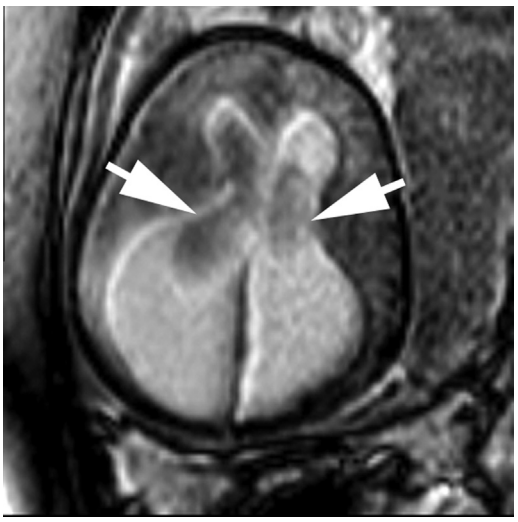

Fig. 4 Intraventricular hemorrhage and ventricular dilatation at 34 weeks gestation. Axial T2-weighted SSFSE image of the brain demonstrates dilatation of the lateral ventricles more evident at the occipital horns. Low signal intensity consistent with hemorrhage is seen within both lateral ventricles (arrows). The dilated ventricles are likely due to obstruction of CSF flow caused by the hemorrhage products.

the fetal brain, images should be obtained with a slice thickness of 3 mm in all 3 orthogonal planes. Examination of the other fetal organs can be performed with a section thickness of 4 mm. To reduce potential signal intensity loss due to cross-talk between sections, it is recommended that SSFSE sequence be acquired in an interleaved fashion with a gap equal to the section thickness [8,10]. Though respiratory triggering is useful in decreasing motion, SSFSE images can be acquired during free maternal breathing too [8]. Due to increase in resolution, smaller field of view (FOV) is preferred in fetal imaging. However, FOV should be adjusted to the increase/decrease in the fetus and/or maternal dimensions, or when aliasing artifact is problematic [8].

Although intravenous gadolinium-based contrast agents have not been found to cause any harm to the fetus [15], these have not been FDA approved for their use during pregnancy. Until the safety of gadolinium-based contrast materials in pregnant patients is established, they are not recommended in fetal MRI. General limitations of fetal MRI include the high cost, limited availability, MRI-specific absolute contraindications such as maternal pacemakers and ferromagnetic implants, and claustrophobia [1,8]. In our experience, claustrophobia is however a minor problem when the patient is adequately instructed and comforted during the examination which typically lasts about 30 min. No maternal sedation or fetal sedation/paralysis is necessary in fetal MRI.

Interpretation of fetal MRI

For proper interpretation of fetal MRI, a radiologist and clinician should be familiar with the normal developing fetal anatomy (Fig. 2). Fetal age (gestational age: GA) is an important factor in the depiction of fetal anatomy. Gestational age is estimated on the basis of the time of the last menstrual period compensated by the measurements on US images in weeks

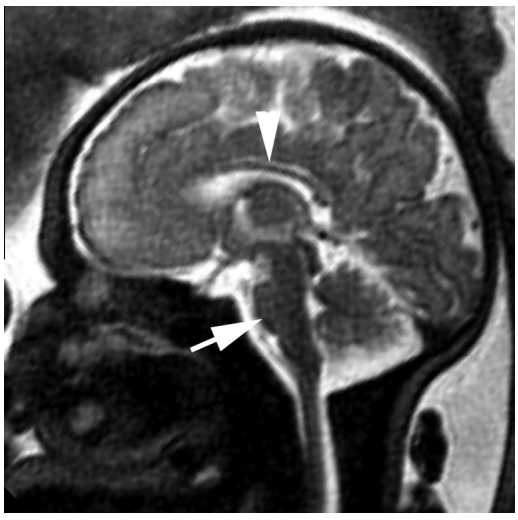

Fig. 5 Normal fetal MRI anatomy of midline structures and posterior fossa. Midline sagittal b-FFE image of normal fetal brain at 34 WG demonstrates the corpus callosum (arrowhead), position of the tentorium cerebelli, normal cerebellar vermis, brainstem with preserved anterior pontine flexure (arrow), and a cisterna magna of less than 10 mm in diameter.

Fig. 6 Cerebellar hypoplasia. Sagittal b-FFE image of a fetal brain at 24 WG shows hypoplastic cerebellum within a normal-sized posterior fossa. Absence of the anterior pontine flexure, resulting in a flat pons (arrow), indicates dysplastic brainstem. Brainstem involvement, a finding that could not be visualized in the ultrasonographic study, worsened the prognosis and outcome expectations of the case.

Fig. 7 Molar tooth sign in Joubert syndrome and related cerebellar disorders (JSRD). Axial b-FFE image of fetal brain at the level of the pontomesencephalic junction at the age of 19 WG shows molar tooth sign (MTS) (arrow) in the form of a thick elongated horizontal superior cerebellar peduncles, and deformed fourth ventricle with increase in its antero-posterior dimension. Note the associated cerebellar hypoplasia with enlarged cisterna magna (arrowhead).

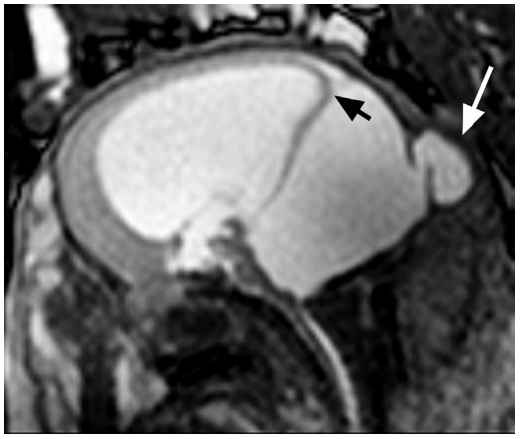

Fig. 8 Dandy Walker malformation. Sagittal b-FFE image of a fetal brain at 26 W shows a markedly enlarged posterior fossa with elevated tentorium cerebelli (black arrow). The large cisterna magna communicates freely with the 4th ventricle due to defective cerebellum. The associated marked hydrocephalus and posterior cephalocele (white arrow) indicate poor postnatal outcome with higher recurrence risk and incidence of chromosomal abnormalities.

(WG: weeks of gestation). Interpretation of fetal MRI is discussed here using a system-oriented approach.

Central nervous system

For convenience, normal and abnormal developing brain is discussed under the following subheadings: cerebral parenchyma, ventricular system and midline structures, and posterior fossa.

Cerebral parenchyma

MRI of the normal fetal cerebrum is characterized initially by the presence of a smooth surface and large ventricles. But as the brain matures the sulci form [16]. Knowledge of the timing of appearance of sulci is important for proper interpretation of

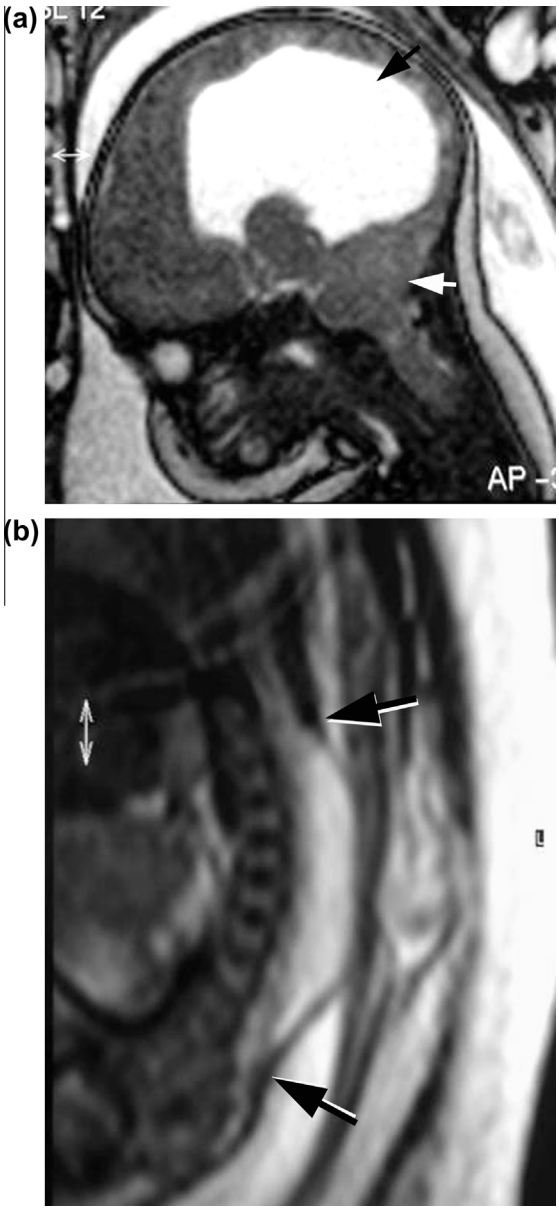

Fig. 9 Chiari II malformation. Sagittal T2-weighted b-FFE images of the head of a fetus at 25 weeks of gestation (a) shows a small posterior fossa (white arrow); obliterated cisterna magna and fourth ventricle; and marked dilatation of the supratentorial ventricles (black arrow). Sagittal T2-weighted b-FFE of the dorsolumbar spine of the same fetus (b) shows associated myelomeningocele between the two black arrows. N.B. The abnormal thickening of the skin of the face and the nuchal fold (black arrowheads) is part of hydrops fetalis caused by associated renal pathology (not shown).

fetal brain development (Fig. 3a) [14]. The sylvian fissure begins to appear at 16 WG; the parieto-occipital and hippocampal sulci begin to appear at 22 WG. The cingular and calcarine begins to appear at 24 WG; the central sulcus start to appear from 26th WG. At 27 WG, the marginal, precentral, postcentral, and superior temporal sulci can be visualized. The superior and inferior frontal sulci appear from the 29th week of gestation. The inferior temporal and collateral sulci are first seen at 33 WG [16]. As early as 34 weeks WG, sulcation is complete and appears similar to that in an adult (Fig. 3b) [8,16,17].

Different layering patterns are observed in fetal brain MRI, depending on the age of the fetus. Early in gestation, cerebral parenchyma is differentiated into three layers: the germinal matrix, the cortical plate, and the intermediate layer. The germinal matrix appears as a dark band that outlines the lateral ventricles on T2-weighted MR images (Fig. 3a). Like the germinal matrix, the cortical plate appears as a dark band on the T2-weighted images and bright on T1-weighted images (Fig. 1). The intermediate zone appears relatively bright on the T2-weighted images, and dark on the T1-weighted images. The multilayered MR pattern of the brain parenchyma corresponds to cellular migration [17]. At 24–27 WG and later, the germinal matrix disappears resulting in the differentiation of only two layers [8,17]. Myelin can be seen at 22–40 WG [12].

Cortical malformations are identified in MRI by noting alteration of the normal sulcation pattern from a fetus particular gestational age. They may be identified as too many sulci in a less mature fetus (as in polymicrogyria), or too few (as in lissencephaly) or abnormally deep or abnormally located sulci (as in schizencephaly) in a more mature fetus [2,8,16]. However, in order for the diagnosis of lissencephaly to be made using MRI, the examination must be undertaken late in pregnancy at least after 30 WG when most of the primary sulci are already present. Thin MR slices should be obtained in several planes so not to miss focal cortical malformations as in schizencephaly [16]. Fetal cerebral parenchymal abnormalities include hemorrhage, gliosis and white matter edema. Hemorrhage in utero does not seem to behave any differently from what is understood postnatally. The good contrast resolution of MRI allows detection of small intraparenchymal hemorrhages. On T1-weighted sequence, hemorrhage can appear as high signal intensity. While T2-weighted sequence may reveal hypointense hemorrhage secondary to intra- or extra-cellular met hemoglobin (Fig. 4) [8]. Gliosis and white matter edema appear as T2-hyperintense and T1-hypointense lesions. DWI will facilitate detection of white matter changes at an earlier stage in a more objective manner [16].

Ventricular system and midline structures

The fetal cerebral lateral ventricles show physiologic disproportionate enlargement of the occipital horns in relation to the frontal horns that remains until 23 WG; thereafter they gradually become smaller [18]. The standard measurement of the cerebral ventricle is obtained in an axial plane through the atrium [18,19]. Ventriculomegaly is diagnosed when the width of atria measures more than 10 mm [18]. Congenital ventriculomegaly is a heterogeneous disease for which genetic, infectious, ischemic, and neoplastic causes have been implicated [20]. Because the prognosis of fetal ventriculomegaly is worse in presence of additional abnormalities, the prenatal detection of such abnormalities is critical [19]. MRI has an important role as an adjunctive tool to sonography in the evaluation of ventriculomegaly; it can rule out the diagnosis, confirm the finding or add associated abnormalities not amenable to sonographic diagnosis. Sonographically-occult findings include developmental abnormalities (such as agenesis of the corpus callosum, cortical malformations, cerebellar dysplasia, Walker–Warburg syndrome, and ponto-cerebellar dysplasia), as well as destructive abnormalities (such as a periventricular leukomalacia, porencephaly and subependymal hemorrhage)

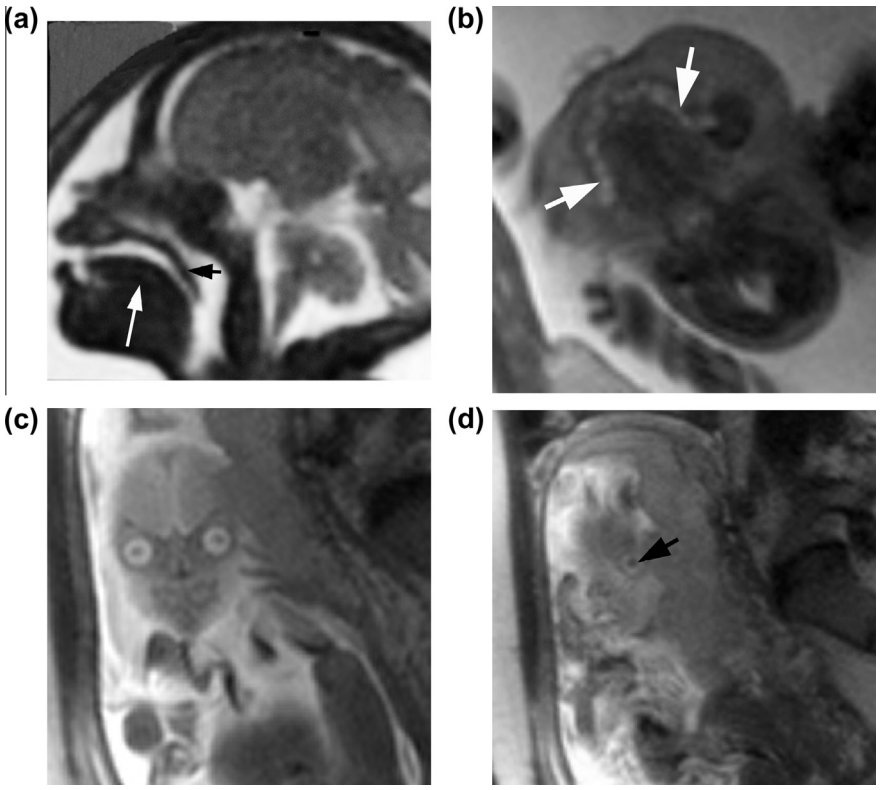

Fig. 10 Fetal face anatomy. Sagittal b-FFE of a fetus at 28 WG (a) shows the amniotic fluid outlining the facial profile. The profile of the tongue (white arrow), nose, lips and chin are well delineated. The palate (black arrow) separates the high intensity fluid in the oral cavity and the hypo-pharynx. Axial T2-weighted SSFSE image (b) of a fetus at 31 WG shows the jaw and the tooth buds (arrows). Coronal T2-weighted SSFSE images at the level of the orbits (c) and more superficially (d) of a fetus at 24 WG show detailed features of the face: eye ball-containing lens (arrow), nose and mouth.

(Fig. 4) [2,8]. Fetal MRI can be helpful in assessing the shape of the entire ventricular system [20]. The margins of the lateral ventricles should be carefully scrutinized for any areas of nodularity that may represent periventricular nodular heterotopias or subependymal tubers in tuberous sclerosis [8].

The corpus callosum can be detected on the midline sagittal T2-WI as a C-shaped hypointense structure at the superior margin of the cavum septum pellucidum [1]. Anomalies of the corpus callosum include hypoplasia, complete or partial agenesis. The midsagittal fetal MR image enables direct visualization of the corpus callosum and diagnosis of complete or partial agenesis anomalies (Fig 5) [8]. Axial and coronal MR images can provide indirect signs of complete agenesis of corpus callosum such as absent cavum septum pellucidum, straight parallel lateral ventricles, dilated occipital horns of lateral ventricles (colpocephaly), high riding third ventricle, and unformed cingulate sulcus [2]. Fetal MRI is useful in diagnosing dysplastic/agenetic septum pellucidum and any associated anomalies related to optic chiasm or pituitary as part of septo-optic dysplasia [19]. Holoprosencephaly is a midline brain anomaly characterized by variable severity of non-cleavage of cerebrum, agenesis of corpus callosum, and associated mid facial anomalies [8].

Posterior fossa

Fetal MRI can determine the global volume of the posterior fossa and show the position of the tentorium cerebelli (Fig. 5). It enables a morphological and biometrical analysis of the posterior fossa structures [20,21]. The cerebellar vermis is best seen on direct midline sagittal and coronal images. The cerebellar hemispheres are best assessed on non-oblique axial and coronal views. Measurements can be made and compared with established norms [8]. Significant reduction of the transverse cerebellar diameter (TCD) is seen in cerebellar hypoplasia. Due to cranio-caudal development of the vermis in embryogenesis, partial agenesis is always inferior. In the presence of a proband, MRI at 20–22 WG is recommended to rule out the possibility of vermian agenesis recurrence. The malformation can affect the vermis or hemispheres and potentially the brainstem. Involvement of the brainstem is diagnosed by the absence of the anterior pontine flexure resulting in a flat pons (Fig. 6) [21]. Joubert syndrome and related cerebellar disorders (JSRD) can be diagnosed by fetal MRI as early as the 17th–18th weeks of gestation by identifying molar tooth sign (MTS) [22]. MTS is s sign that results from a combination of midbrain, vermian, and superior cerebellar peduncle abnormalities (Fig. 7) [23]. However, in all of the previously discussed cases, the posterior fossa is normal in size and the tentorium cerebelli is in the correct position [21].

The cisterna magna is an important landmark in the posterior fossa. Detection of an enlarged cisterna magna (> 10 mm) should prompt a detailed examination of the fetal brain [22]. Dandy Walker continuum describes a spectrum of anomalies of the posterior fossa that are diagnosed by an enlarged cisterna magna and include: mega cisterna magna (normal 4th ventricle, vermis and tentorium); Blake's pouch cyst (cystic

Fig. 11 Craniofacial deformity associated with holoprosencephaly. Mid-sagittal b-FFE in a fetus at 34 WG shows a profoundly small head results in frontal sloping and abnormal face profile in this fetus with holoprosencephaly (semilobar). Note the abnormal anterior fusion of cerebral hemispheres, partial anterior agenesis of the corpus callosum (arrowhead), and inferior vermian hypoplasia (arrow).

dilatation of the 4th ventricle, normal vermis, and normal tentorium); vermian hypoplasia (cystic dilatation of the 4th ventricle, hypoplastic vermis, and normal tentorium); and Dandy-Walker malformation (DWM) (cystic dilatation of the 4th ventricle, hypoplastic vermis, and superior displacement of the tentorium) (Fig. 8) [19–21,24].

Obliteration of the cisterna magna is the most consistent finding in Arnold-Chiari malformation. The most common forms of Chiari malformation are the types I and II. Chiari I consists of downward herniation of the cerebellar tonsils. In Chiari II, the posterior fossa is small with herniation of the inferior part of the vermis and fourth ventricle, hypoplastic cerebellar hemispheres and usually supratentorial ventricular dilatation. Obliteration of the cisterna magna should suggest a spinal defect as myelomeningocele is always associated with Chiari II malformation (Fig. 9) [20,22,23].

Spine

The entire length of the fetal spine could be studied in multiple planes on MRI. Evaluation of the spinal column is thus important to detect abnormalities such as neural tube defects (NTDs). NTD are a heterogeneous group of malformations resulting from failure of normal neural tube closure early in embryologic development. NTD include anencephaly, cephalocele, spina bifida, and less commonly iniencephaly [9,25]. Spina bifida is a defect of the vertebrae resulting in exposure of the contents of the neural canal. Similarly, cephaloceles are diagnosed when contents protrude through a skull defect. MRI shows well the location and extent of the bony defect as well as the size and contents of the protruding sacs. [19,21].

Face and neck

The fetal face is an important part of antenatal structural survey. Facial malformation may indicate an underlying chromosome abnormality or syndrome [26–28]. Three-dimensional US technique has been used to generate accurate detailed images of the facial surface anatomy [26]. Using the three orthogonal planes, MRI can help US in assessment of complex craniofacial deformities such as holoprosencephaly and craniosynostosis (Figs. 10 and 11) [29]. MRI enables visualization of the internal anatomy including the oral and hypo-pharynx. The fetal airway is fluid-filled and therefore appears bright on T2-weighted images (Fig. 10a). Because of possible life threat-

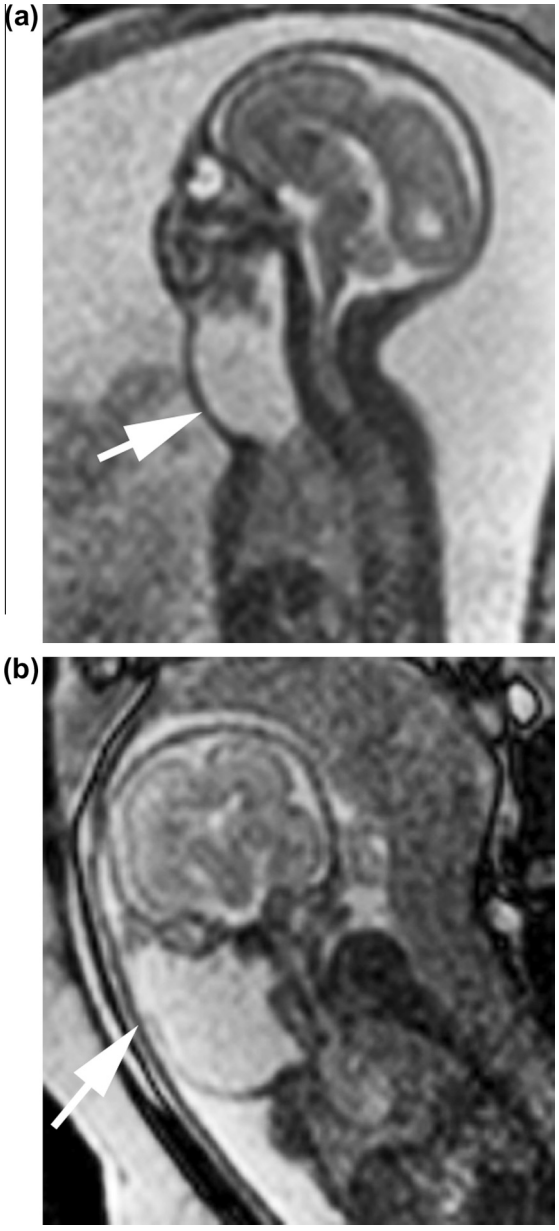

Fig. 12 Cystic mass in the anterior neck region. Sagittal (a) and coronal (b) b-FFE images of a fetus at 20 WG show a large cystic mass (arrow) is seen on the anterior and right anterolateral aspect of the neck extends from the floor of the mouth to the thoracic inlet. The mass is cystic with no evidence of solid components or septa. Medial proximity of the mass to the airway is noted with no evidence of displacement or obstruction. Chromosomal studies indicted Turner syndrome. The expectant parents opted termination of pregnancy. Autopsy indicated infiltrative cystic hygroma.

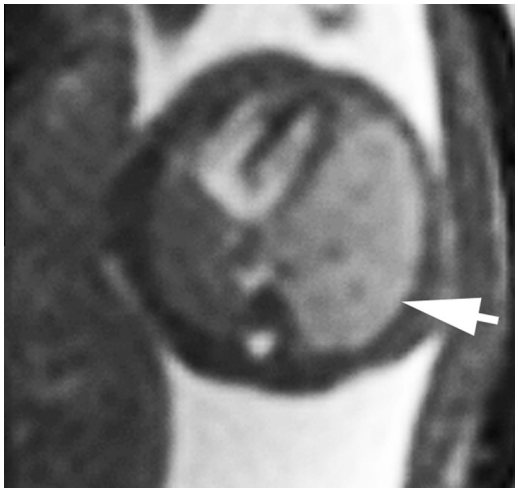

Fig. 13 Cystic adenomatoid malformation (CCAM). Axial b-FFE image of the thorax of a fetus at 24 WG demonstrates homogeneous moderately high signal intensity involving the left lung representing Microcystic (CCAM type III) (arrow). The mass displaces the heart and mediastinal structures to the right side.

ening airway obstruction, the identification of neck masses in utero is crucial determinant of method and location of delivery. MRI demonstrates the relationship of the masses to the neck, airway and mediastinum [26]. This has been of emerging importance as the ex utero intrapartum treatment (EXIT) and fetal surgery are increasingly being used to manage these fetuses [27]. The most common fetal neck masses are teratomas and goiters, anteriorly, and cystic hygromas, posterolaterally [26]. MRI is useful in differentiating goiter form other anterior neck masses (e.g. teratoma and hemangioma) because of the characteristic signal intensity of the thyroid being hyperintense on T1- and isointense on T2-weighted images. Ultrasonography is the modality of choice for diagnosis of cystic hygromas in-utero; however, fetal MRI can be useful in assessment of infiltration of the cysts into the surrounding structures (Fig. 12) [26–28]. The differential diagnosis of an extracranial cystic mass in the posterior neck region includes cystic hygroma or meningo-encephalocele [3,26]. A prerequisite for the diagnosis of encephalocele in contrast to nuchal cystic hygroma is the demonstration of an associated bony defect in the skull and protrusions of the brain. MRI provides exquisite detail of both the cranial defect and the herniated contents [24,25].

Thorax

The normal fetal lungs have homogeneous moderately high signal intensity on T2-weighted images. With increasing maturation, the fetal lungs show increase in volume and in T2-signal. Sagittal and coronal images at the level of the diaphragm clearly show the distinction between the structures of the thorax and those of the abdomen [29]. The most common masses within the fetal chest are congenital cystic adenomatoid malformation (CCAM), broncho-pulmonary sequestration, congenital diaphragmatic hernia (CDH), and hydrothorax. Congenital chest masses have characteristic MR appearances. On fetal MRI, CCAM appearance varies depending on whether the lesions are microcystic or macrocystic (Fig. 13) [30]. CCAM may consist of few large cysts (type I) or more numerous smaller to moderate sized cysts (type II) of increased T2-signal intensity arising from any lung lobe. Microcystic CCAM (type III) typically demonstrates homogeneous moderately high signal intensity on T2-weighted signal that could be indistinguishable from bronchopulmonary sequestration in the absence of a visible feeding artery from the aorta to suggest the diagnosis of sequestration [30,31]. CDH occurs most commonly in the posterior aspect of the left hemi-diaphragm due to failure of formation of the diaphragmatic leaflets. The presence of liver in the chest in fetuses with left sided CDH markedly worsens the prognosis. MRI allows direct visualization of the position of the liver and differentiates meconium-filled herniated bowel loops form cystic lesions within the chest [3,32]. Assessment of fetal lung development with MRI has been particularly pertinent to the management of conditions as chest masses in which prognosis is closely related to the severity of pulmonary hypoplasia. Marked

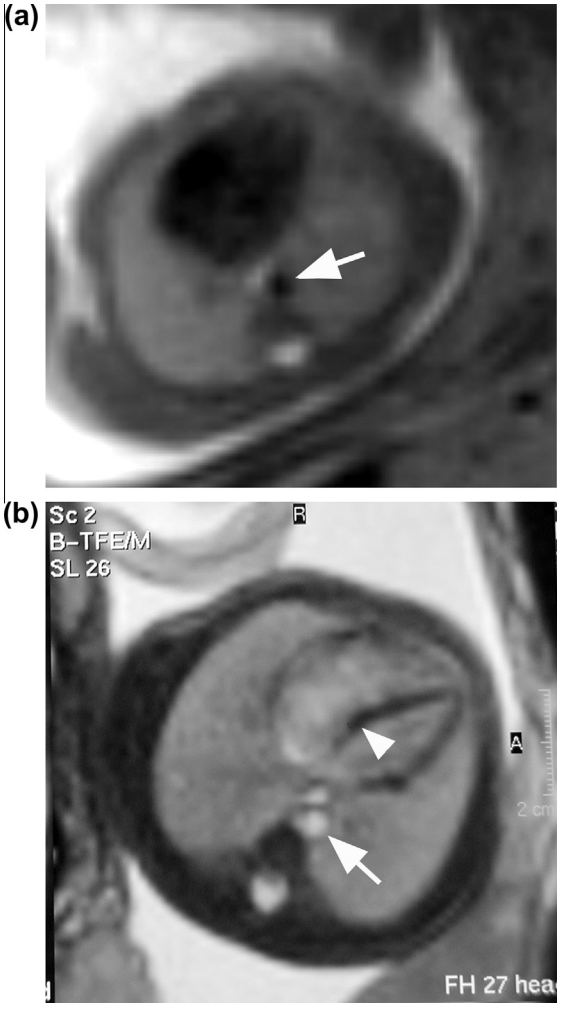

Fig. 14 Normal MRI appearance of fetal cardiovascular structures at 29 WG. Axial T2-weighted SSFSE image of the thorax (a) shows the heart and aorta (arrow) as signal void structures; no cardiac details could be depicted. On Axial b-FFE image at the same level (b), the aorta (arrow) and heart have high signal intensity delineating the cardiac ventricular morphology and interventricular septum (arrowhead).

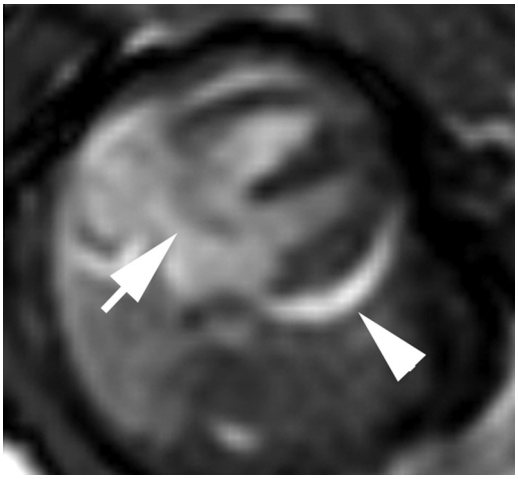

Fig. 15 Atrioventricular canal defect. Axial b-FFE image in a 30 weeks' gestation fetus shows enlarged heart with evident large atrioventricular septal defect (arrow) and pericardial effusion (arrowhead).

reduction of signal intensity as well as lung volumes are characteristic MR findings in fetuses with pulmonary hypoplasia [31].

It is complicated to visualize the fetal heart with MRI owed to its small size and high pulsation rate. Depicting fetal heart and vessels depend on the MR sequence used (Fig. 14). With SSFSE T2-weighted images, the heart and vessels are demonstrated as flow void that contrasts well with the hyperintense surroundings [30]. Balanced steady state free precession sequences, as true-FISP or b-FFE, are superior in visualizing the heart and vessels demonstrated as hyperintense structures. MRI protocol for studying the fetal heart along body and cardiac planes has been introduced recently [11]. Fetal MRI shows potential value in detecting cardiac abnormalities without the need of sedation or fetal cardiac gating. Fetal MRI can identify positional anomalies of the heart, cardiac malformations associated with cardiomegaly, different sizes of the cardiac chambers, and cardiac tumors. Malformations of the great vessels and atrioventricular canal defects can be visualized in larger fetuses by fetal MRI (Fig. 15) [33]. More studies are needed to develop fetal MRI cardiac triggering and advance dynamic sequences needed for evaluation of the anatomical and functional aspects of fetal cardiac pathologies.

Abdomen and gastrointestinal tract

On T2-weighted images of fetal abdomen, organs such as the esophagus, stomach, intestine, urinary collecting systems,

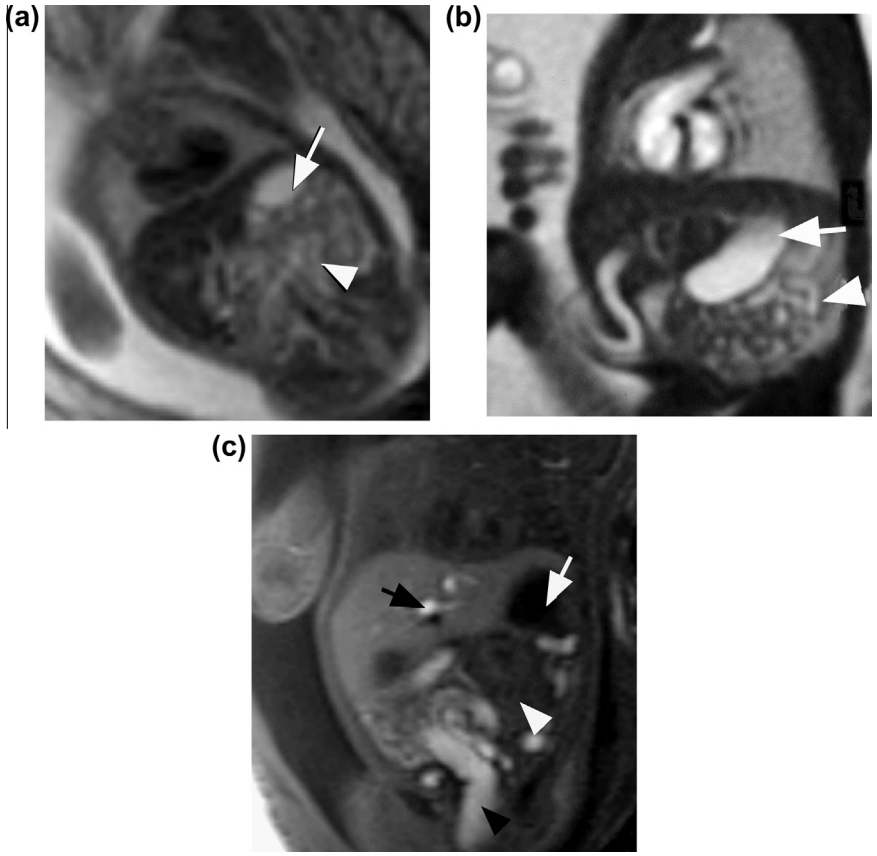

Fig. 16 Normal fetal abdomen. MRI of a fetus abdomen at 27 WG using coronal T2-weighted SSFSE sequence (a), coronal oblique T2-weighted b-FFE (b), and T1-weighted Turbo FLASH sequence (c). On T2-weighted images (a and b), the liver is hypointense; the fluid in the stomach (arrows) and small bowel (arrowheads) has high signal intensity. Note that the bowel loops are seen better in (b) than in (a); b-FFE is less prone to motion artifacts caused by fetal bowel peristalsis. On T1-weighted image (c), the liver is moderately hyperintense; the fluid in the stomach (white arrow) and small bowel (white arrowhead) is hypointense. The meconium in the colon and rectum is hyperintense (black arrowhead). The high signal intensity of the hepatic vessels (black arrow) is caused by the unsaturated blood within.

and bladder appear hyperintense because of the fluid they contain [29]. The meconium is produced after 13 WG and slowly migrates from small bowel to colon. Due to functional obstruction of the anal canal at 20 WG, meconium progressively accumulates in the bowel. The proximal intestine appears hyperintense on T2- and hypointense on T1- weighted images being formed mainly of ingested amniotic fluid. The colon contains meconium with high protein and minerals content; it appears hypointense on T2- and hyperintense on T1-weighted images [29,30,34]. Identification of meconium in the colon on T1-weighted images can aid in the diagnosis of complex fetal abnormalities (Fig. 16) [34]. The bowel diameters increase with advancing age. At 20 WG small bowel measures 2–3 mm and large bowel 3–4 mm in diameter. By 35 WG, small bowel measures 5–7 mm and large bowel 8–15 mm in diameter [32]. Through recognition of the caliber and signal changes of small and large bowel, MRI can diagnose bowel atresia and locate the level of bowel obstruction with widely dilated bowel loops proximal to the site of stenosis [30]. On MRI, abdominal organs, and meconium-filled extracorporeal small intestines can be identified in gastroschisis and omphalocele (Fig. 17) [30,34,35].

Early in fetal life the majority of erythropoiesis occurs in the fetal liver. The liver shows high signal on T1- and low signal on T2-weighted images secondary to increased iron content from fetal hemoglobin; protein, copper, and zinc likely contribute to the increased T1-signal intensity of the liver [29,30,36]. The spleen is detectable by 20 WG; it shows homogeneous signal that decreases with advancing gestation on T2-weighted images [29,37]. The gall bladder, a cystic structure under the lower aspect of the live, could be demonstrated from 18 WG onward. The biliary ducts cannot usually be demonstrated under normal conditions [32]. Fetal MRI can assess cystic masses related to the liver. The differential diagnosis of an intrahepatic cyst includes congenital liver cyst, choledochal cyst, biliary atresia or duodenal duplication. Congenital hepatic cyst is usually unilocular and, unlike choledochal cyst, does not communicate with the biliary system (Fig. 18) [37,38].

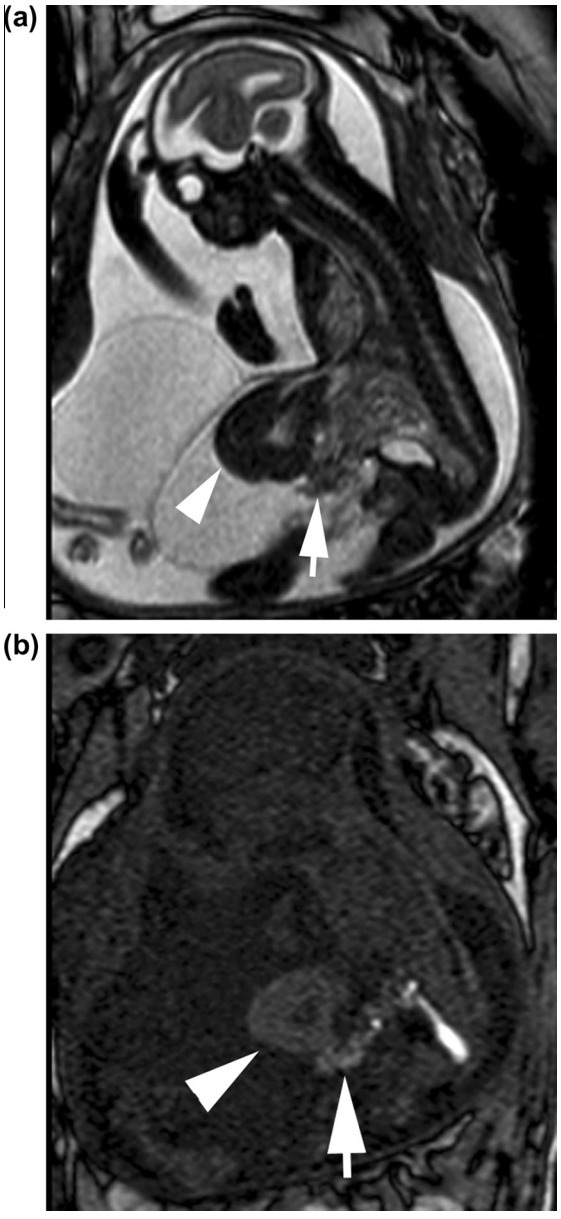

Fig. 17 Omphalocele. Sagittal b-FFE (a) of a fetus at 23 WG shows the liver (arrowhead) and other soft tissues (arrow) to be extra-abdominal within a fluid-filled sac (omphalocele). Sagittal T1-weighted GRE (b) aids in characterization of the herniating organs: the high signal intensity liver (arrowhead) and the meconium filled intestine (arrow).

Fig. 18 Giant intra-hepatic cyst. Sagittal b-FFE image of a fetus at 34 WG shows a large unilocular cyst related to the right hepatic lobe (arrow) that does not communicate with the biliary system. The cyst is separate from the urinary bladder (arrowhead). The cyst enlarged rapidly and an elective caesarean section was done at the age of 38 WG. The newborn was operated upon at the age of 2 days and a large hepatic cyst was removed.

Genitourinary system

The length, signal intensity on T2-weighted images, and apparent diffusion coefficient (ADC) of the fetal kidney change significantly with gestational age [39]. Renal cortex is hypointense to the medulla on T2-weighted images. Progressive increase in renal cortex/medulla signal intensity ratio with gestational age reaches its maximum at term [39,40]. The urinary bladder is easily recognized as a fluid-filled structure in the pelvis. Since the fetal pelvis is very small, the filled urinary bladder may occupy considerable portions of the abdomen in older fetuses (>30 WG) (Fig. 19) [30]. MRI can show morphological features of urinary diseases as cystic lesions of the kidneys (Fig. 20), obstructive uropathy (e.g. posterior urethral valve) (Fig. 21), renal tumors, and urinary tract anomalies [40]. Though differentiation of renal cysts from a dilated collecting system can sometimes be difficult, central cystic lesions are more likely to be dilatation of the collecting system, whereas lesions at the periphery are more likely to be renal cysts [40,41]. The dysplastic fetal renal parenchyma shows increased signal intensity on T2-weighted images produced by cystic dilatation of the collecting tubules [30,40]. A helpful clue to the diagnosis of a dysplastic kidney is missing of the normal bright signal on ADC images of DWI [41]. The scrotum and penis are often recognized in the male fetus. MRI proved to be an excellent technique for revealing different fetal genital diseases as ovarian cysts and hypo-/epi-spadia [40]. MRI aids also in assessment of the fetal perineum which is helpful in the fetuses with cloacal exstrophy and in cases in which gender is an important consideration for diagnosis [33,40,41].

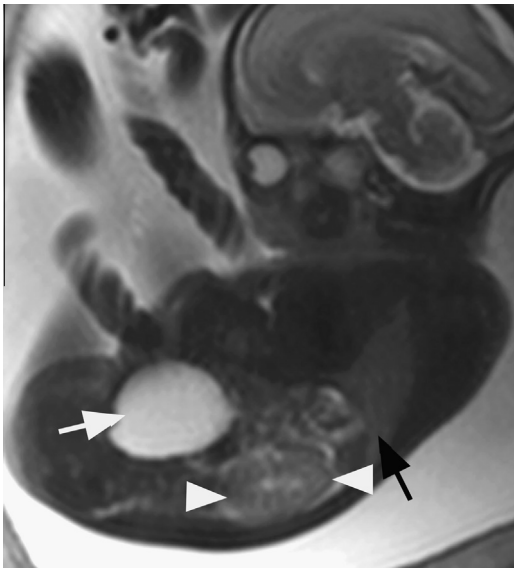

Fig. 19 MRI appearance of normal fetal kidneys. Sagittal T2-SSFSE of a fetal abdomen at 25 WG: Note the size and the signal appearance of the normal kidney between the two arrowheads. The fluid-filled urinary bladder (white arrow), the adequate volume of the amniotic fluid, and the developing lungs (black arrow) indicate good renal function. Note that the urinary bladder can occupy a considerable portion of the abdomen as a normal finding.

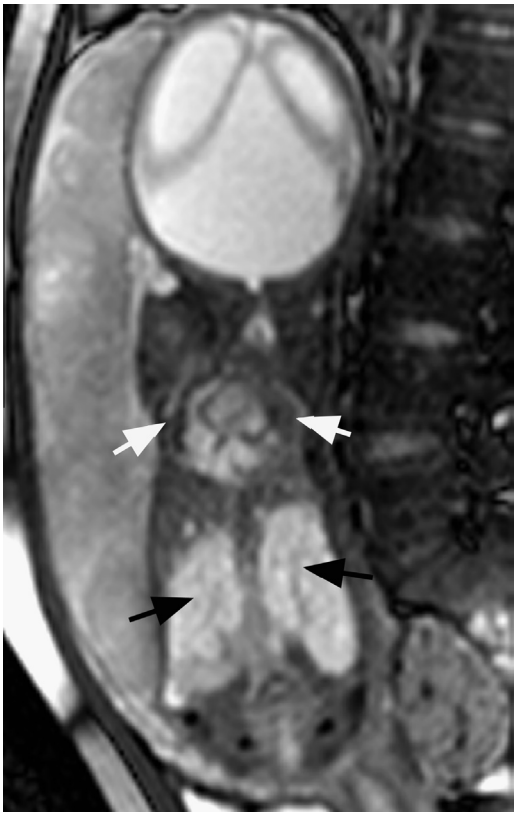

Fig. 20 Bilateral polycystic kidneys. Coronal b-FFE of a fetus at 28 WG shows bilateral renal enlargement (black arrows). The generalized increase of the signal intensity of renal parenchyma is produced by cystic dilatation of the collecting tubules. Both lungs (white arrows) appear as thin dark strips at each side of the hyperintense heart. Absence of urinary bladder, marked reduction of amniotic volume (oligohydraminos), and hypoplastic lungs are indications of a lethal outcome. Marked hydrocephalus is also associated in this case of Meckel–Gruber syndrome. N.B. Ultrasonographic examination was inadequate in this case due to marked oligohydraminos.

Musculoskeletal system and fetal organ volume

Fetal MRI can assess the skeleton and muscles owed to the innovations in MRI sequence technology such as echoplanar imaging (EPI), thick slab T2-Weighted, and dynamic sequences. Ultrasonography, particularly three-dimensional imaging, remains the method of choice in measuring bones and observing abnormal fetal skeletal anomalies such as club foot or abnormal fingers [29]. Fetal MRI can help in diagnosing complex musculoskeletal abnormalities through careful assessment of the whole fetus and detection of associated abnormalities [41]. Echoplanar MR imaging (EPI) are useful to obtain an overview of thoracic size and skeletal development [32]. MRI can detect fetal surface contours, and assess the integrity of the body wall [2]. Fetal MRI can estimate organ volumes such as lung volume which enables prediction

Fig. 21 Posterior urethral valve. Sagittal b-FFE of a fetus at 29 WG shows dilated urinary bladder and posterior urethra proximal to obstruction by a posterior urethral valve. The obstructed urinary bladder and urethra assume a (key-hole appearance). Note the associated oligohydramnios.

of outcome in fetuses at risk for pulmonary hypoplasia especially in the third trimester of pregnancy [31,42,43].

Pregnancy-related structures

Evaluation of the placenta, umbilical cord and amniotic sac is part of the fetal MR examination. The T2-weighted MR images show the placenta as a moderately hyperintense structure. Prenatal MRI of the normal placenta shows morphological changes during gestation (Fig. 22). At 19–23 WG, placenta has regular homogeneous structure. With advanced gestation, placenta shows increase in lobules number and T2-signal intensity. The placenta/amniotic fluid signal ratio significantly decreases with advanced gestation. Moreover, the visual difference between the inner lobular and homogeneous placental tissue are increasingly marked with ongoing placental maturation [44]. During the placental aging, venous stasis and/or thrombotic changes may cause areas of normal placental infarctions that appear as map-like changes [45,46]. Multiplanar MR images allow detailed assessment of placental insertion defects and tumors that can guide better management [47]. The umbilical cord and its insertion are also well demonstrated in MRI [48,49].

Amniotic fluid abnormality, whether deficient (oligohydraminoms) or in excess (polyhydraminos), is usually the first clue of an underlying fetal disorder. The amniotic fluid has a low signal on T1-weighted and a high signal on T2-weighted images [48]. MRI is useful in the assessment of pregnancies complicated by oligohydramnios, which can limit the diagnostic sensitivity of US [50,51].

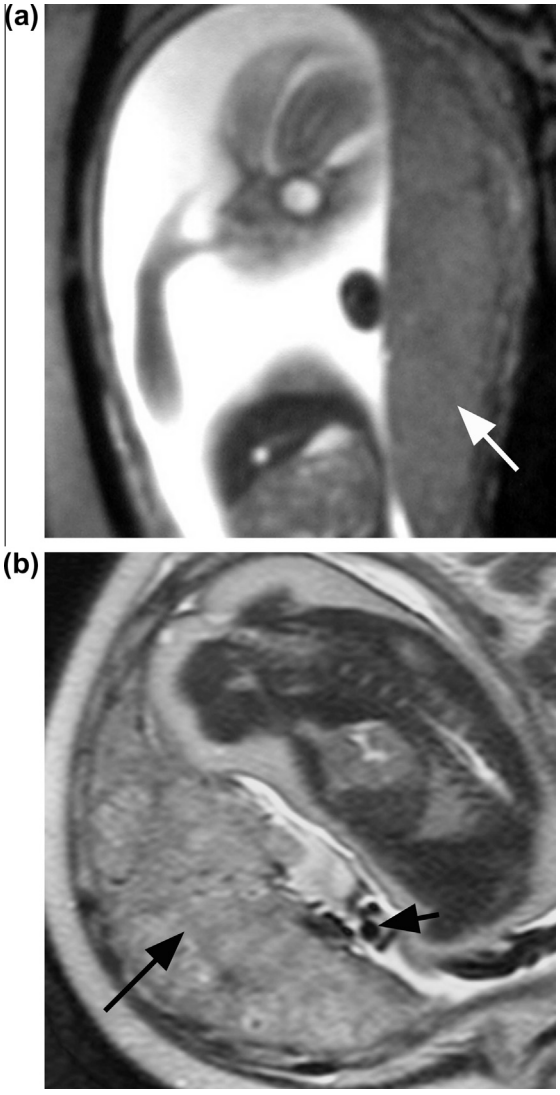

Fig. 22 Normal morphological changes of the placenta. T2-weighted MR image (a) of a gravid uterus at 22 WG reveals the regular homogeneous placental structure at this age (arrow). At 32 WG (b), the placental structure (arrow) shows increased signal intensity, heterogeneity and lobulations. The short arrow points to the cross section of the three-vessel umbilical cord: two equal-sized umbilical arteries and a larger umbilical vein.

Role of fetal MRI in prenatal counseling of fetal anomalies

Prenatal counseling helps the family to decide between prenatal therapies, postnatal therapies or the interruption of the pregnancy [52]. Through accurate demonstration of the fetal disorder, prenatal MRI can play a role in determination pregnancy prognosis and management. The additional findings provided by MRI are helpful to expectant parents and their clinicians in understanding the severity of the abnormality and reaching an informed decision regarding pregnancy continuation or termination [22,25,53].

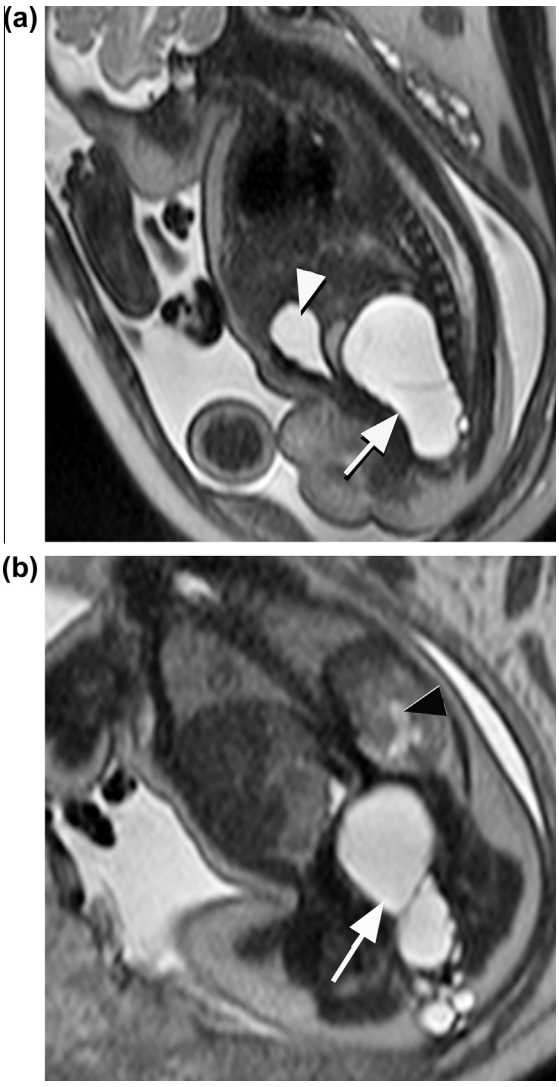

Fig. 23 The impact of fetal MRI on management of sacrococcygeal teratoma. Sagittal (a) and coronal (b) T2-weighted SSFSE images of a fetus at 32 WG show a large pelvi-abdominal mass (arrows). The mass is multicystic; it has homogenous low signal on T1-(not shown) and high signal on T2-weighted images. Absence of solid components, hemorrhage or vessels suggests a benign lesion. Note that the mass is totally intra-fetal which favors a vaginal delivery rather than a caesarean section. The mass compresses the urinary bladder (white arrowhead) and causes hydronephrosis (black arrowhead). Fetal urinary tract affection suggests earlier date of delivery. Multiplanar evaluation of the tumor helps too in postnatal surgery planning.

Role of fetal MRI in supporting in-utero surgery

Fetal MRI can facilitate management decisions and guide therapy when fetal surgery is a consideration or when delivery is expected to present unique challenges [54,55]. Conditions in which fetal MRI appears to contribute to fetal surgical planning and postoperative evaluation include congenital diaphragmatic hernia, cystic adenomatoid malformation, myelomeningocele, complicated twin pregnancies, upper airway obstruction, and sacrococcygeal teratoma [3,54,55]. Sacrococcygeal teratoma is the most common congenital neoplasm; its high perinatal mortality and morbidity rates seem to be related to the content and extent of the mass rather than to its size [56,57]. The impact of fetal MRI on the management of sacrococcygeal teratoma is discussed as an example (Fig. 23). Fetal MRI provides important multiplanar images that may obviate the need for early postnatal imaging [4]. MR images are more easily understood by surgeons and other clinicians resulting in more accurate prenatal counseling and improved preoperative planning for surgical resection [58].

Role of fetal MRI in supporting research studies

In addition to the clinical indications, MRI is used in research studies of normal and abnormal human fetal development [59].

Research studies of MRI of normal fetuses at different gestational ages allow establishing of normative measures that can be used in early identification of developmental abnormalities [22,60,61]. The significant technical progress in fetal MRI sequences, such as Diffusion Tensor imaging and functional MRI, as well as the capability of formation of 3-D images may open the door for future studies of fetal development and gene therapy [14,62–64].

Conclusions

MRI allows excellent detailed visualization of the fetus in utero as well as the pregnancy structures. By using a systematic approach, fetal MRI is useful in the recognition of the developing fetal anatomy, detection of subtle fetal abnormalities and evaluation of complex lesions. Prenatal MRI can facilitate management decisions and guide therapy, particularly when fetal surgery is a consideration or when delivery is expected to present unique challenges.

Conflict of interest

The author has declared no conflict of interest.

Compliance with Ethics Requirements

The author declares no potential conflicts of interest with respect to the manuscript authorship, and/or publication of this article. The author received no financial support for the manuscript authorship and/or publication of this work. No ethical approval was required for preparation and publication of this article by Institute's Medical Research Ethics Committee (REC).

References

[1] Levine D. Ultrasound versus magnetic resonance imaging in fetal evaluation. Top Magn Reson Imaging 2001;12:25–38.
[2] Simon EM, Goldstein RB, Coakley FV, Filly RA, Broderick KC, Musci TJ, et al. Fast MR imaging of fetal CNS anomalies in utero. AJNR Am J Neuroradiol 2000;21:1688–98.
[3] Frates M, Kumar A, Benson C, Ward V, Tempany C. Fetal anomalies: comparison of MR imaging and US for diagnosis. Radiology 2004;232:398–404.
[4] Miller E, Ben-Sira L, Constantini S, Beni-Adani L. Impact of prenatal magnetic resonance imaging on postnatal neurosurgical treatment. J Neurosurg 2006;105(3 Suppl):203–9.

[5] American College of Radiology (ACR), Society for Pediatric Radiology (SPR). ACR-SPR practice guideline for the safe and optimal performance of fetal magnetic resonance imaging (MRI). [online publication]. Reston (VA): American College of Radiology (ACR); 2010. p. 10 [cited 2010 October 1] Available from: <http://www.guidelines.gov/content.aspx?id=32509>.
[6] Stecco A, Saponaro A, Carriero A. Patient safety issues in magnetic resonance imaging: state of the art. Radiol Med 2007;112:491–508.
[7] Kanal E, Borgstede JP, Barkovich AJ, Bradley WG, Etheridge S, Felmlee JP, et al. American college of radiology white paper on MR safety. AJR Am J Roentgenol 2002;178: 1335–47.
[8] Glenn OA, Barkovich AJ. Magnetic resonance imaging of the fetal brain and spine: an increasingly important tool in prenatal diagnosis, Part 1. AJNR Am J Neuroradiol 2006;27:1604–11.
[9] Adzick NS, Thom EA, Spong CY, Brock 3rd JW, Burrows PK, Johnson MP, et al. A randomized trial of prenatal versus postnatal repair of myelomeningocele. N Engl J Med 2011;364(11):993–1004.
[10] Yamashita Y, Namimoto T, Abe Y, Takahashi M, Iwamasa J, Miyazaki, et al. MR imaging of the fetus by a HASTE sequence. AJR Am J Roentgenol 1997;168:513–9.
[11] Saleem SN. Feasibility of magnetic resonance imaging (MRI) of the fetal heart using balanced steady-state-free-precession (SSFP) sequence along fetal body and cardiac planes. Am J Roentgenol AJR 2008;191:1208–15.
[12] Chung HW, Chen CY, Zimmerman RA, Lee KW, Lee CC, Chin SCc. T2-Weighted Fast MR imaging with true FISP versus HASTE comparative efficacy in the evaluation of normal fetal brain maturation. AJR Am J Roentgenol 2000;275:1375–80.
[13] Girard N, Fogliarini C, Viola A, Confort-Gouny S, Le Fur Y, Viout P, et al. MRS of normal and impaired fetal brain development. Eur J Radiol 2006;57:217–25.
[14] Kasprian G, Brugger PC, Weber M, Krssak M, Krampl E, Herold C, et al. In utero tractography of fetal white matter development. Neuroimage 2008;43:213–24.
[15] Webb JA, Thomsen HS, Morcos SK. The use of iodinated and gadolinium contrast media during pregnancy and lactation. Eur Radiol 2005;15:1234–40.
[16] Garel C. The role of MRI in the evaluation of the fetal brain with an emphasis on biometry, gyration and parenchyma. Pediatr Radiol 2004;34:694–9.
[17] Brisse H, Fallet C, Sebag G, Nessmann C, Blot P, Hassan M. Supratentorial parenchyma in the developing fetal brain: *in vitro* MR study with histologic comparison. AJNR Am J Neuroradiol 1997;18:1491–7.
[18] Bowerman RA, Nyberg DA. Normal fetal anatomic survey. In: Nyberg D, McGahan J, Pretorius D, Pilu G, editors. Diagnostic imaging of fetal anomalies. Philadelphia: Lippincott Williams & Wilkins; 2003. p. 1–30.
[19] Prayer D, Brugger PC, Nemec U, Milos RI, Mitter C, Kasprian G. Cerebral malformations. In: Prayer D, editor. Fetal MRI. Berlin: Springer-Verlag; 2011. p. 287–308.
[20] Guibaud L. Practical approach to prenatal posterior fossa abnormalities using MRI. Pediatr Radiol 2004;34:700–11.
[21] McGahan JP, Pilu G, Nyberg D. Cerebral malformations. In: Nyberg D, McGahan J, Pretorius D, Pilu G, editors. Diagnostic imaging of fetal anomalies. Philadelphia: Lippincott Williams & Wilkins; 2003. p. 220–90.
[22] Saleem SN, Zaki MS. Role of magnetic resonance imaging (MRI) in prenatal diagnosis of pregnancies at risk for joubert syndrome and related cerebellar disorders (JSRD). Am J Neuroradiol AJNR 2010;31(3):424–9.
[23] Saleem SN, Zaki MS, Soliman NA, Momtaz M. Prenatal MRI diagnosis of molar tooth sign at 17–18 weeks of gestation in two fetuses at risk for Joubert Syndrome and related cerebellar disorders. Neuropediatrics 2011;42:35–8.
[24] Malinger G, Lev D, Lerman-Sagie T. The fetal cerebellum. Pitfalls in diagnosis and management. Prenat Diagn 2009;29:372–80.
[25] Saleem SN, Said AH, Abdel-Raouf M, El-Kattan E, Zaki MS, Madkour N, Shokry M. Fetal MRI in the evaluation of fetuses referred for sonographically suspected neural tube defects (NTDs): impact on diagnosis and management decision. Neuroradiology 2009;51(11):761–72.
[26] Benacerraf B, Nyberg D. The face and neck. In: Nyberg D, McGahan J, Pretorius D, Pilu G, editors. Diagnostic imaging of fetal anomalies. Philadelphia: Lippincott Williams & Wilkins; 2003. p. 335–79.
[27] Kathary N, Bulas DI, Newman KD, Schonberg RL. MRI imaging of fetal neck masses with airway compromise: utility in delivery planning. Pediatr Radiol 2001;31:727–31.
[28] Poutamo J, Vanninen R, Partanen K, Ryynanen M, Kirkinen P. Magnetic resonance imaging supplements ultrasonographic imaging of the posterior fossa, pharynx and neck in malformed fetuses. Ultrasound Obstet Gynecol 1999;13:327–34.
[29] Nemec SF, Brugger PC, Kasprian G, Nemec U, Graham Jr JM, Prayer D. The skeleton and musculataure. In: Prayer D, editor. Fetal MRI. Berlin: Springer-Verlag; 2011. p. 235–46.
[30] Shinmoto H, Kashima K, Yuasa Y, Tanimoto A, Morikawa Y, Ishimoto H, et al. MR imaging of non-CNS fetal abnormalities: a pictorial essay. Radiographics 2000;20:1227–43.
[31] Kasprian G, Balassy C, Brugger P, Prayer D. MRI of normal and pathological fetal lung development. Eur J Radiol 2006;57:261–70.
[32] Brugger PC. MRI of fetal abdomen. In: Prayer D, editor. Fetal MRI. Berlin: Springer-Verlag; 2011. p. 361–401.
[33] Saleem SN. Fetal cardiac magnetic resonance (CMR), echocardiography – new techniques. Gani Bajraktari (Ed.), ISBN: 978-953-307-762-8, InTech; 2012;10:167–84. Available from: <http://www.intechopen.com/articles/show/title/fetal-cardiac-magnetic-resonance-cmr->.
[34] Farhataziz N, Engels J, Ramus R, Zaretsky M, Twickler D. Fetal MRI of urine and meconiul by gestational age for the diagnosis of genitourinary and gastrointestinal abnormalities. AJR Am J Roentgenol 2005;184:1891–7.
[35] Hertzberg B, Nyberg D, Neilsen I. Ventral wall defects. In: Nyberg D, McGahan J, Pretorius D, Pilu G, editors. Diagnostic imaging of fetal anomalies. Philadelphia: Lippincott Williams & Wilkins; 2003. p. 507–46.
[36] Duncan KR, Baker PN, Gowland PA, Isaa B, Moore R, Worthington B, et al. Demonstration of changes in fetal liver erythropoiesis using echo-planar magnetic resonance imaging. Am J Physiol 1997;273, G965-7.
[37] Brugger PC, Prayer D. Fetal abdominal magnetic resonance imaging. Eur J Radiol 2006;57:278–93.
[38] Kim MJ, Park YN, Han SJ, Yoon CS, Yoo HS, Hwang EH, Chung KS. Biliary atresia in neonates and infants: triangular area of high signal intensity in the porta hepatis at T2-weighted MR cholangiography with US and histopathologic correlation. Radiology 2000;215(2):395–401.
[39] Witzani L, Brugger P, Hormann M, Kasprian G, Csapone-Balassy C, Prayer D. Normal renal development investigated with fetal MRI. Eur J Radiol 2006;57:294–302.
[40] Caire JT, Ramus RM, Magee KP, Fullington BK, Ewalt DH, Twickler DM. MRI of fetal genitourinary anomalies. AJR Am J Roentgenol 2003;181:1381–5.
[41] Amin RS, Nikolaidis P, Kawashima A, Kramer LA, Ernst RD. Normal anatomy of the fetus at MR imaging. Radiographics 1999;19, p. S201–S214.
[42] Hassibi S, Farhataziz N, Zaretsky M, McIntire D, Twickler D. Optimization of fetal weight estimates using MRI: comparison of acquisitions. AJR Am J Roentgenol 2004;183:487–92.

[43] Cannie M, Jani JC, Keyzer FD, Devlieger R, Schoubroeck DV, Witters I, et al. Fetal body volume: use at MR imaging to quantify relative lung volume in fetuses suspected of having pulmonary hypoplasia. Radiology 2006;241(3):847–53.
[44] Blaicher W, Brugger PC, Mittermayer C, Schwindt J, Deutinger J, Bernaschek G, et al. Magnetic resonance imaging of the normal placenta. Eur J Radiol 2006;57:256–60.
[45] Sepulveda W, Sebire N, Harris R, Nyberg D. The placenta, umbilical cord and membranes. In: Nyberg D, McGahan J, Pretorius D, Pilu G, editors. Diagnostic imaging of fetal anomalies. Philadelphia: Lippincott Williams & Wilkins; 2003. p. 85–132.
[46] Palacios Jaraquemada JM, Bruno C. Magnetic resonance imaging in 300 cases of placenta accreta: surgical correlation of new findings. Acta Obstet Gynecol Scand 2005;84:716–9.
[47] Palacios Jaraquemada JM, Bruno C. Gadolinium-enhanced MR imaging in the differential diagnosis of placenta accreta and placenta percreta. Radiology 2000;216(2):610–1.
[48] Werner H, Daltro P. Molar pregnancy. < http://www.thefetus.net/page.php?id = 1699 > [Accessed 2.03.06].
[49] Leung AKC, Robson WLM. Single umbilical artery: a report of 159 cases. Am J Dis Child 1989;143:108–11.
[50] Hill L, Sohaey R, Nyberg D. Abnormalities of amniotic fluid. In: Nyberg D, McGahan J, Pretorius D, Pilu G, editors. Diagnostic imaging of fetal anomalies. Philadelphia: Lippincott Williams & Wilkins; 2003. p. 59–84.
[51] Poutamo J, Vanninen R, Partanen K, Kirkinen P. Diagnosing fetal urinary tract abnormalities: benefits of MRI compared to ultrasonography. Acta Obstet Gynecol Scand 2000;79:65–71.
[52] Sharma G, Heier L, Kalish R, Troiano R, Chasen S. Use of fetal magnetic resonance imaging in patients electing termination of pregnancy by dilation and evacuation. Am J Obstet Gynecol 2003;189(4):990–3.
[53] Hengstschläger M. Fetal magnetic resonance imaging and human genetics. Eur J Radiol 2006;57:312–5.
[54] Coakley FV. Role of magnetic resonance imaging in fetal surgery. Top Magn Reson Imaging 2001;12(1):39–51.
[55] Farmer D. Fetal surgery. Br Med J 2003;326:461–2.
[56] Danzer E, Hubbard AM, Hedrick HL, Johnson MP, Wilson RD, Howell J, et al. Diagnosis and characterization of fetal sacrococcygeal teratoma with prenatal MRI. AJR Am J Roengenol 2006;187(4), W350-6.
[57] Altman RP, Randolph JG, Lilly JR. Sacrococcygeal teratoma: American Academy of Pediatrics Surgical Section Survey-1973. J Pediatr Surg 1974;9:389–98.
[58] Coakley FV, Hricak H, Filly RA, Barkovich AJ, Harrison MR. Complex fetal disorders: effect of MR imaging on management—preliminary clinical experience. Radiology 1999;213:691–6.
[59] Glenn OA. MR imaging of the fetal brain. Pediatr Radiol 2010;40:68–81.
[60] Saleem SN. Fetal magnetic resonance imaging (MRI): a tool for a better understanding of normal and abnormal brain development. J Child Neurol; 2013 May 3. [Epub ahead of print] doi:http://dx.doi.org/10.1177/0883073813486296.
[61] Zaki MS, Abdel-Aleem A, Abdel-Salam G, Marsh S, Silhavy J, Barkovich AJ, Ross M-E, et al. The molar tooth sign: a new Joubert syndrome and related cerebellar disorders classification system tested in Egyptian families. Neurology 2008;70(7):556–65.
[62] Brugger PC. Methods of fetal MRI. In: Prayer D, editor. Fetal MRI. Berlin: Springer-Verlag; 2011. p. 65–80.
[63] Jardri R, Pins D, Houfflin-Debarge V, Chaffiotte C, Rocourt N, Pruvo JP, et al. Fetal cortical activation to sound at 33 weeks of gestation: a functional MRI study. Neuroimage 2008;42:10–8.
[64] Lancaster MA, Gopal DJ, Kim J, Saleem SN, Silhavy JL, Louie CM, et al. Defective Wnt-dependent cerebellar midline fusion in a mouse model of Joubert syndrome. Nat Med 2011;17(6):726–31.